

ANALYSIS OF DOUBLE RESISTANCE SPOT WELDING'S FAILURE IN HIGH STRENGTH LOW ALLOY STEEL

Hayder H. Khaleel^{1,2*}, Ibtihal A. Mahmood¹, Fuad Khoshnaw³

¹Mechanical Engineering Department, University of Technology, Baghdad, Iraq

²Engineering Technical College / Najaf, Al- Furat Al-Awsat Technical University, 31001 Al-Najaf, Iraq

³De Montfort University, Leicester, United Kingdom

* me.19.32@grad.uotechnology.edu.iq

High strength low alloy steel (HSLA DOCOL 500 LA) is utilized in the automotive structure because of its superior qualities such as good fatigue resistance, a high strength-to-weight ratio, assisting in reducing the weight of the vehicle, increasing fuel efficiency and lower CO₂ emissions. Resistance Spot Welding (RSW) is the most welding technique that is used to join automobile parts together. This study investigated the RSW process for high-strength steel. By utilizing the Taguchi approach, the optimization process for double spot nuggets with the principal welding parameters of welding current, welding time, and electrode force was carried out. The values of optimum parameters were 8800Amp for welding current, welding time of 30 cycles and 2560 N for electrode force. Mechanical and microstructure tests were carried out to study the failure modes while the fatigue test was achieved to obtain the fatigue endurance limit and it was at a maximum load 1500 N and during the fatigue test two types of failure happened: full pull-out failure and cracks around the nugget zone.

Keywords: high strength low alloy steel (HSLA), resistance spot welding, taguchi method, fatigue life, microhardness

1 INTRODUCTION

Resistance spot welding (RSW) is the main welding technique that used in the automotive sector. Vehicle body-in-white can contain thousands of resistance spot welding joints [1]. RSW joints are crucial during car crashes because they help keep welded sheets together and absorb impact energy [2-4]. It is a complex technique that includes electrical, mechanical and metallurgical effects on the welded structure. Under pressure created by two electrodes formed of copper alloys, the components in RSW are joined [5]. Four distinct stages of RSW can be identified. The force applied by the electrodes during the "squeeze" time forces the metal parts mechanically together. During the "weld" stage, an electrical current flows, melting the metal and forming a weld pool in the process. For the duration of the "hold" phase, the current is cut off. The heat is removed from the interface, lowering the temperature as a result; typical cooling rates range from 2000 to 4000 K/s. The weld pool solidifies, forming a weld nugget. The electrodes are finally released during the "off" period. [6]. The RSW process is schematically shown in Fig.1.

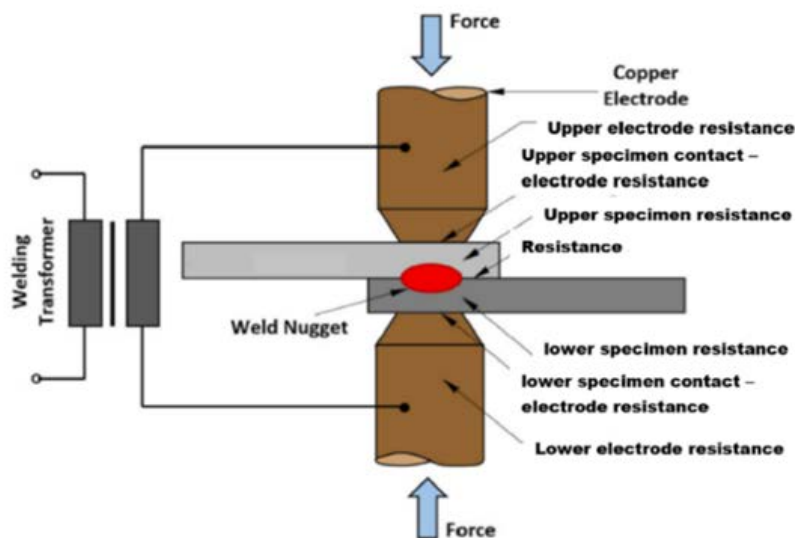


Fig. 1. Schematic of RSW process [7]

The main benefit of RSW is that it is easy to automate, not expensive to install welding machines and it can use for a wide range of materials such as high-strength steel, aluminum and low carbon steel [8-11]. Electrode force, welding time, welding current, and sheet thickness are all factors that affect RSW, but the welding current is by far the most crucial factor [12].

Overload failure and fatigue failure are the two main categories of spot weld failure phenomenon. Accidents, unpaved roads, or driving circumstances that place an excessive amount of strain on the vehicle are just a few

situations where overload failure may occur. There are two types of overload failure which are interfacial failure and pullout failure [13,14]. The interfacial failure happens when the crack propagates through the weld nugget and the material shows brittle failure. When the spot nugget separates from the sheets, the material fails in a ductile manner, which indicates a high amount of absorbed energy [15,16]. The phenomenon of the fatigue failure in engineering components has become one of the most important issues [17,18].

Due to its benefits, such as a high strength-to-weight ratio, the automotive industry widely used high strength steel. Many papers studied RSW for various materials. Chakkaravarthi Rajarajan et al. used Response surface methodology (RSM) to optimize the process parameters of (RSW) for advanced high strength steel (AHSS) joints that are used in the manufacture of thin-walled automotive structural frames. According to ANOVA, welding current, electrode pressure, and time all had a significant impact on the weld joints [19].

Jiazhuang Tian et al. studied the microhardness and fatigue life for parts made of Q&P1180 steel welded by resistance spot welding and laser spot welded. In welded zone they noticed lath martensite with high microhardness value. The fatigue limit for resistance spot welding was about 91% of fatigue limit for laser spot welding. The fatigue failure occurred between nugget zone and heat affected zone because of stress concentration in this regions [20].

S. K. Hussein and O.S. Barrak conducted RSW for two metals, AISI 304L and AA 6061-T6, with various thicknesses. The design of experiments was used to examine the effects of three welding parameter values. The findings demonstrated that increasing the sheet thickness and welding current sheet thickness raised the strength of the welded components. Strength of welded parts decreased as electrode force and welding time were increased [21].

In contrast to past studies, which focused on a single area, the current work proposes a double RSW optimization strategy for high strength steel low alloys (DOCOL 500 LA). Taguchi method optimization was used to figure out the best welding parameters, including current of welding, time of welding, and electrode force. One of the best ways for the optimization process is the Taguchi approach, which can minimize the number of tests by rearranging the experiments into an orthogonal array and choosing the most efficient parameters. In order to assess the mechanical characteristics of weld nuggets and analyze overload failure, tensile shear tests and microhardness tests were conducted, and a fatigue test was useful in investigating fatigue failure. Additionally, microstructure tests were conducted to examine how the three welding zones which are the fusion zone (FZ), the heat-affected zone (HAZ), and the base material(BM) were influenced by the welding conditions.

2 METHODOLOGY

2.1 Material

This work was completed using HSLA steel (DOCOL 500 LA) supplied by the SSAB company for the production of steel. Due to its superior qualities, including a good fatigue resistance and high strength-to-weight ratio, this type of steel has recently been utilized extensively by automobile manufacturers. The sheets had a 0.8 mm thickness. Thermo ARL 3460 Optical Emission Spectrometer was used to analyze the chemical composition. Table 1 lists the outcomes of the HSLA's actual chemical composition.

Table 1. HSLA chemical composition (wt%)

C%	Mn%	S%	Si%	Cr%	P%	Mo%	Ni%	Cu%	Al%	Fe%
0.092	1.33	0.006	0.39	0.034	0.016	0.006	0.035	0.008	0.004	Bal.

The microstructure for HSLA was studied before and after the resistance spot welding using Optical Microscopy (Olympus BXM51). Using ImageJ software, the base material's average grain size was determined to be about 3.9 μ m, as shown in Figs. 2 and 3, respectively. It was discovered that the base material's microstructure has an equiaxed grain structure and is largely ferritic.

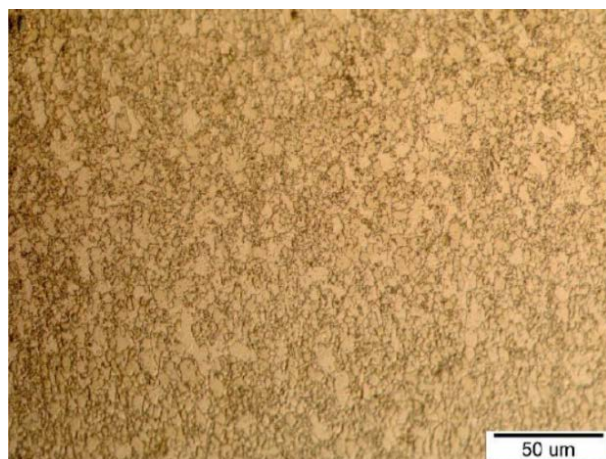


Fig. 2. The microstructure of base material

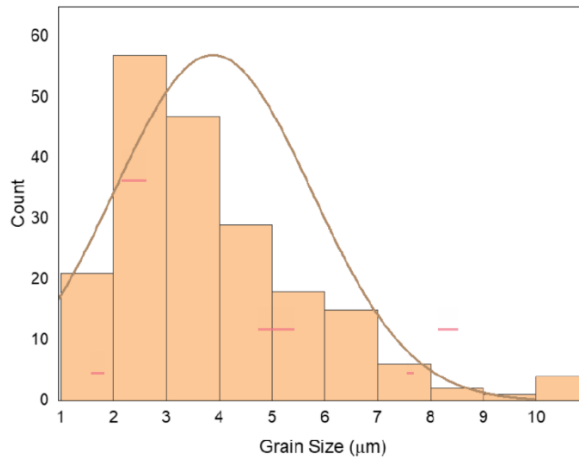


Fig. 3. The grain size distribution of the base material

with a 50 kN maximum capacity and 2 mm/min strain rate, a tensile test was performed in accordance with ASTM-E8 for metallic materials sheet type to determine the mechanical properties. The test machine was connected to a computer. The tensile test specimens are shown in Fig.4 both before and after the test.

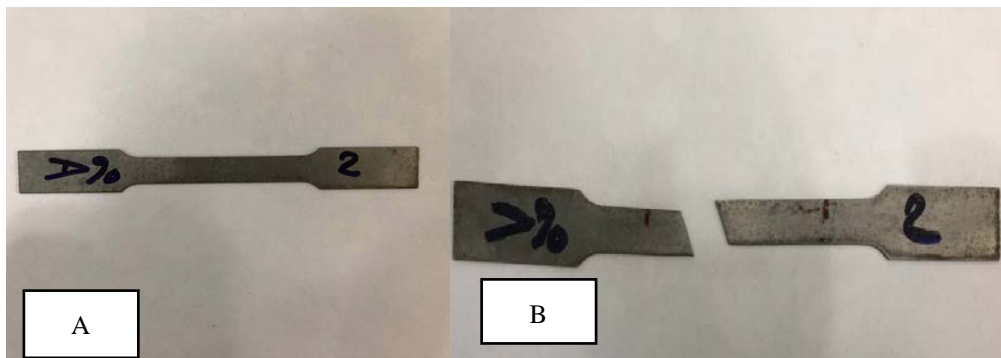


Fig. 4. Tensile test specimen A. before test. B. after test.

The mechanical properties of HSLA steel that obtained from tensile test listed in table 2 below.

Table 2. Tensile Test Result

Strength of the Yield (MPa)	Strength at Maximum Tension (MPa)	Strength to Fracture (MPa)	Elongation %
549	691	677	23

2.2 Welding Process

The resistance spot welding process was achieved for samples with two nuggets of 6 mm for each and their dimensions were selected according to ISO standards where the overlap region dimensions (45x45) mm as shown in Fig. 5.

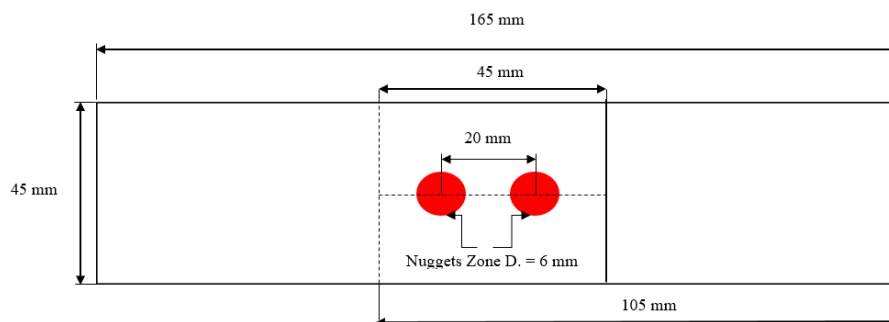


Fig. 5. Dimensions of spot welding sample

In order to remove any contaminations and guarantee high-quality welding, the samples were first prepared using a CNC machine and then cleaned with synthetic acetone. The WIMTOUCH 1800 digital spot welding machine was used to complete the welding process. The machine was connected to a compressor to produce the necessary electrode force and was cooled by a water system. The American Welding Society (AWS) standards were followed when choosing the copper alloys for the electrode tip, which had a 6 mm diameter. To hold the samples in the proper orientation, a unique fixture was created. The welding machine's control unit, as depicted in Fig. 6, could change the amount of current, force, and welding time.

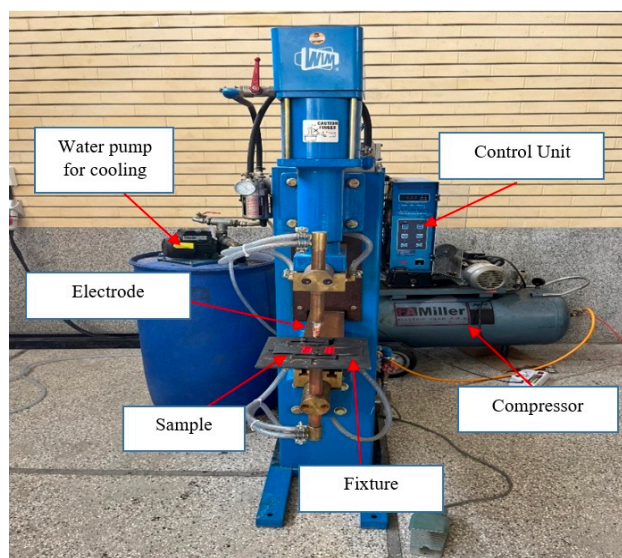


Fig. 6. Spot welding Machine

A visual measuring machine, which was calibrated and connected to a computer to get a precise measurement of nugget diameter as illustrated in Fig.7, was used to calculate the area of spot and nugget diameters for each specimen after welding.

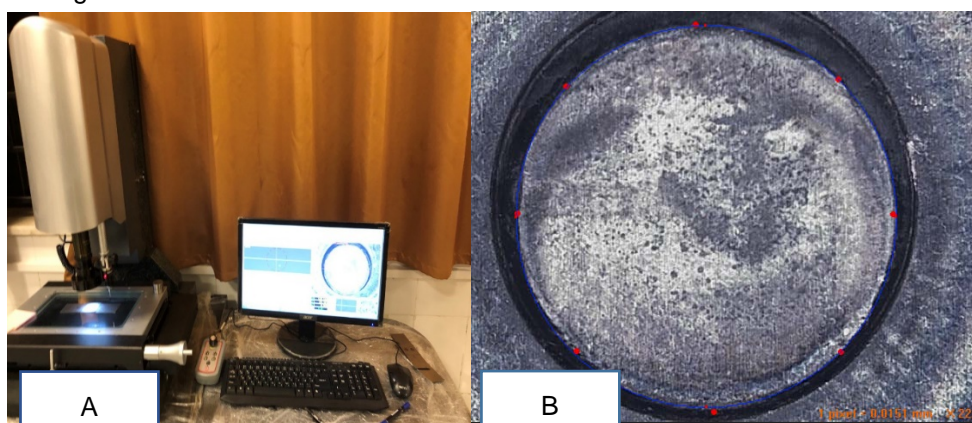


Fig. 7. (A) visual measuring device (B) Top view of RSW

2.3 Experiment design.

In order to determine the perfect tensile shear strength and to analyze the type of failure that occurred, three welding parameters were selected for this work. These parameters included three levels for each of the time of welding, current of welding, and electrode force. The AWS specifications for high strength steels products with maximum tensile strengths ranging from 350 MPa to 700 MPa guided the selection of these levels [22]. The parameters were examined using the L9 array, the Taguchi method, and Minitab 19 [23]. Table 3 includes a list of the L9 orthogonal array welding parameters and levels.

Table 3. L9 orthogonal array

Trial	Current of Welding (Amp)	Time of Welding (cycle)	Electrode Force (N)
1	5700	9	1900
2	5700	20	2230
3	5700	30	2560
4	7250	9	2230
5	7250	20	2560
6	7250	30	1900
7	8800	9	2560
8	8800	20	1900
9	8800	30	2230

As shown in Fig. 8, nine parts were welded to assess the absorbed energy, tensile shear force and to identify the mode of failure.

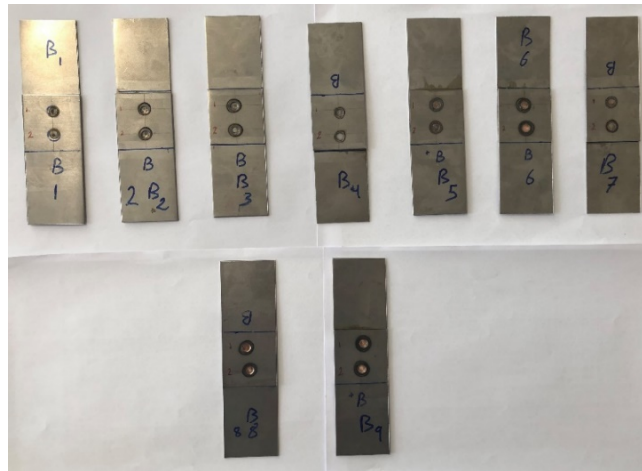


Fig. 8. Spot welded samples

2.4 Tensile-Shear Test

Tensile shear testing was done after the welding process and after measuring the nuggets' diameter. The test was completed using the SANTAM STD-600 tensile test machine as shown in Fig.9. The experiments were conducted twice, with the average result used, to increase the accuracy of the results of the tensile shear test with a strain rate of 1 mm/min. Maximum tensile shear force was obtained from this test and also the maximum absorbed energy which was measured as the area under the curve of load-displacement up to the peak load and obtained as the difference between two displacements multiplied by the corresponding tensile force [24].



Fig. 9. Tensile Shear Test

2.5 Microhardness Tests

A microhardness test was conducted to investigate the impact of welding parameters on the mechanical properties for the sample welded with optimum welding parameters. Vickers microhardness measurements were made for three regions of the spots welds: FZ, HAZ, and BM horizontally across the cross-section of the welded sample as shown in Fig.10.

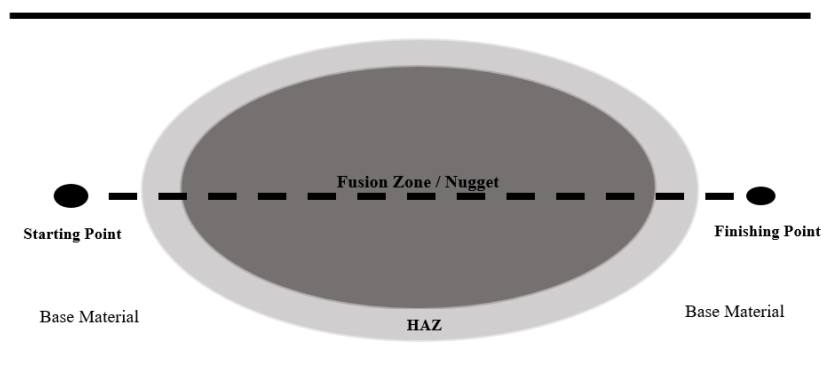


Fig. 10. The path of microhardness measurements across the weld cross-section

Prior to welding, the base metal had an average microhardness of 206 3 HV. As part of the sample preparation, samples were ground and polished in accordance with ASTM E90-82. The test was conducted as depicted in Fig. 11 with a load of 500 gf and a dwell time of 10 s.

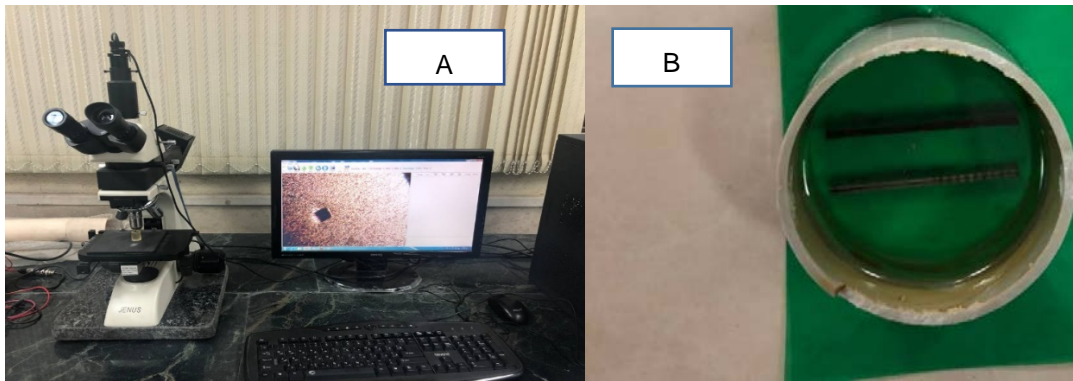


Fig. 11. (A) Microhardness test device (B) Microhardness sample

2.6 Fatigue Test

The fatigue test was carried out using the fatigue machine INSTRON 8802 with a maximum capacity of 250 kN. The machine was connected to the computer to analyze the data obtained from the machine. The machine first calibrated and then started the test with a frequency 10 Hz and stress ratio (R=0.1). The start load was 15000 N until reach 1 million cycles which presents the endurance limit as shown in Fig.12.

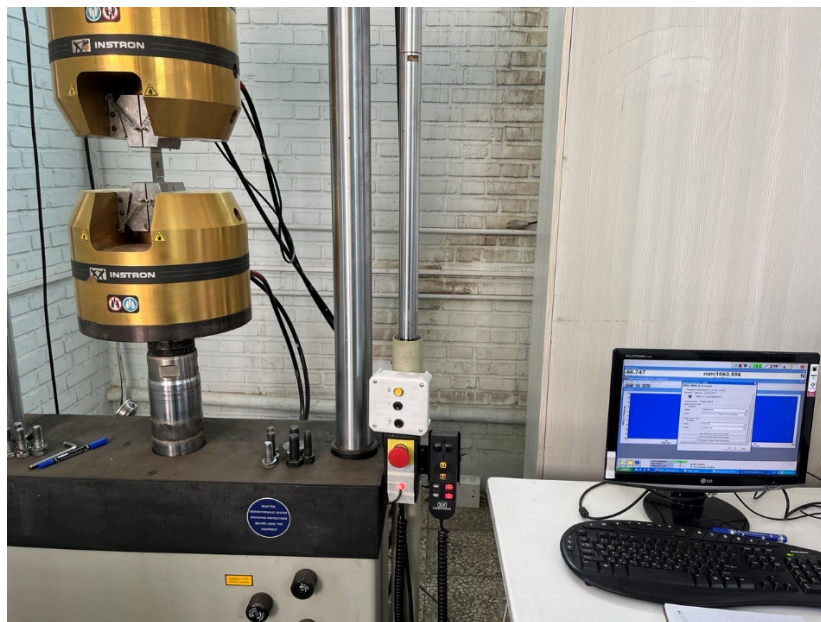


Fig. 12. Fatigue Test

3 RESULTS AND DISCCSIONS

3.1 Tensile Shear Results.

After the spot welding process was completed and formed the spot nugget, the diameters of these nuggets were measured and then the tensile shear test was done. The results can be listed in table 4.

Table 4. Results of Tensile Shear Test

Trial	Current for welding. (Amp)	Time of Welding (cycle)	Electrode Force (N)	Force of Shear (N)	Absorbed Energy (J)	Diameter of the First Nugget (mm)	Diameter of the Second Nugget Diameter (mm)
1	5700	9	1900	11537	16.37	5.80	6.17
2	5700	20	2230	12665	24.08	6.12	6.31
3	5700	30	2560	11821	12.13	6.33	6.32
4	7250	9	2230	12675	20.57	6.62	6.38
5	7250	20	2560	17256	40.13	7.13	6.94

Trial	Current for welding. (Amp)	Time of Welding (cycle)	Electrode Force (N)	Force of Shear (N)	Absorbed Energy (J)	Diameter of the First Nugget (mm)	Diameter of the Second Nugget Diameter (mm)
6	7250	30	1900	15559	26.94	6.67	6.82
7	8800	9	2560	15706	33.77	6.57	6.47
8	8800	20	1900	15147	31.98	6.76	6.71
9	8800	30	2230	18158	46.23	7.16	6.90

Fig.13 shows the load-displacement curve which obtained from the tensile shear test for the nine samples by taking the mean results for the two attempts of each trial in order to increase the accuracy of the outcomes. It can be seen that the curve has linear behavior before reach to the peak and after that start to fail. The tensile shear force increased by increasing the welding current up to a maximum force 18158 N in trial 9 and this indicates that the current of welding is the most effective parameter among the welding parameters.

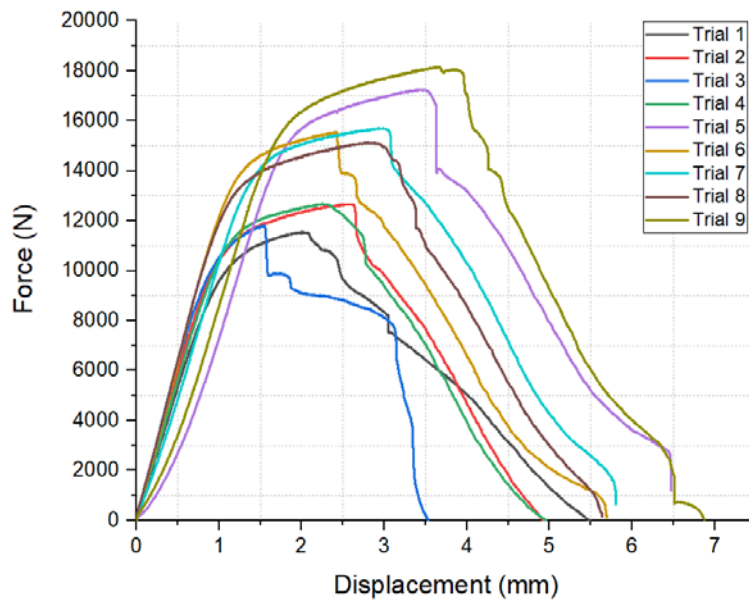


Fig. 13. Load-displacement curve

Fig.14 illustrates the tensile shear force vs. absorbed energy. It could be observed that absorbed energy is also increased by increasing tensile shear force due to increasing the welding current and the maximum absorbed energy was 46.23 J for trial 9. Fig.15 shows the tensile force vs. area of the two nuggets and it could be noticed the difference in nugget areas.

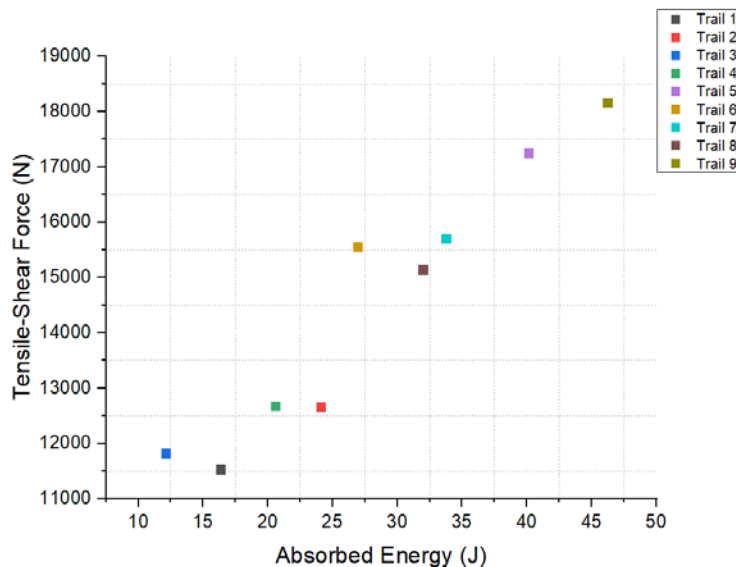


Fig. 14. Tensile-Shear force vs. Absorbed Energy

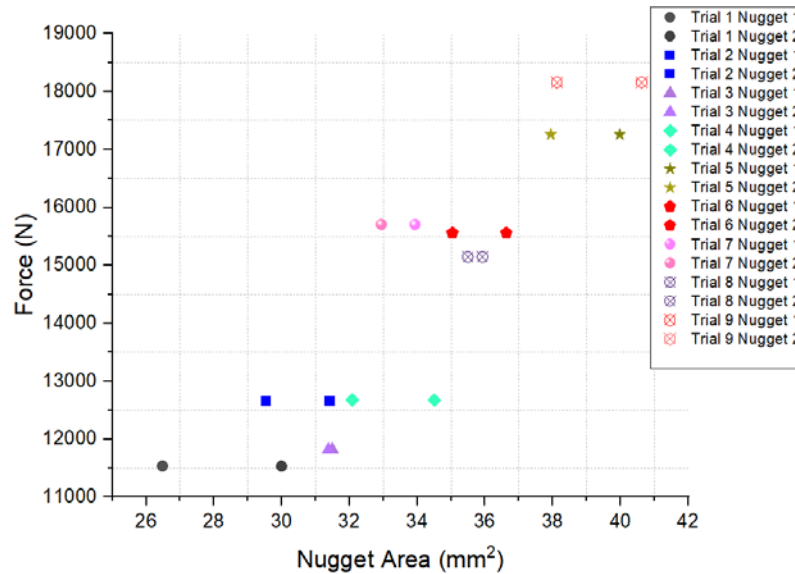


Fig. 15. Tensile-Shear force vs. area of the nuggets

The shunt effect phenomenon is the cause of the difference between the first nugget diameter and the second nugget diameter as shown in Figs.14 and 15 respectively. In fact, if the nuggets are placed closely together due to electric current shunting, the previous welds may affect the subsequent nugget. The previously created nugget may cause the welding current to deviate from its intended course. Therefore, it's possible that the current or current density is insufficient to produce a weld of good quality.

To figure out the optimal welding current, welding time, and electrode force, as well as to determine the contribution ratio for each welding parameter, all of these data were analyzed using the Taguchi method using Minitab 19 software. The best welding current, according to the Taguchi method was 8800 Amp, the optimum welding time was 30 cycles, and the optimum electrode force was 2560 N. Fig.16 illustrates the main effect plot produced by Minitab software.

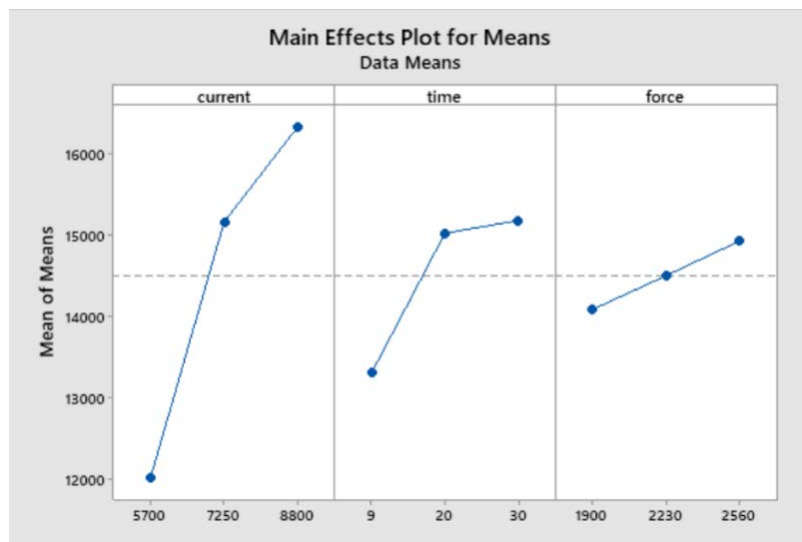


Fig. 16. Main effect plot

The confirmation test was also carried out. The main goal of this test is to compare the experimental results of tensile shear force for a sample welded with obtaining optimum values of welding parameters with the predicted value that was presented by Minitab software. The predicted value for Taguchi's optimum parameters is 17010 N. The outcomes of the confirmation test on two samples are displayed in Fig.17. The result of the first sample was 16814 N with a 1.1% error rate, while the final result of the second sample was 15529 N with an error rate of 8.1% and a variation of 7.8%.

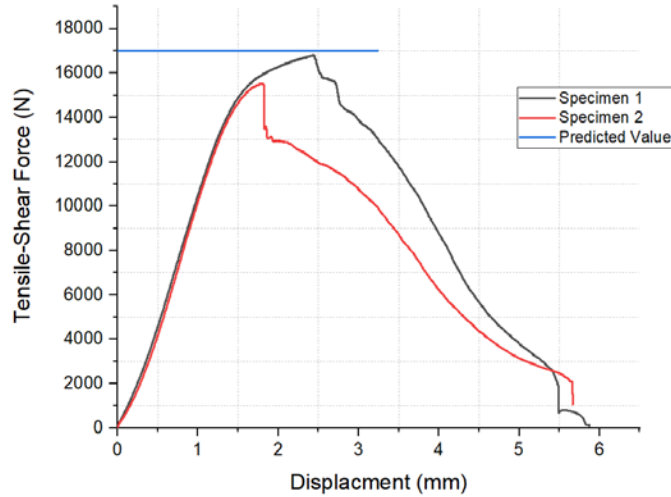


Fig. 17. Result of the confirmation test

Studying the impacts of welding parameters on the output outcomes and their statistically significant influences, as indicated in table 5, is the primary goal of the ANOVA that was obtained from Minitab. Welding current was the most efficient characteristic, followed by welding duration and electrode force.

Table 5. ANOVA result

Source	DF	Seq SS	Adj SS	Adj MS	F	P	Contribution ratio %
current	2	30078853	30078853	15039426	3.35	0.230	64.51
time	2	6480867	6480867	3240433	0.72	0.581	13.9
force	2	1075317	1075317	537658	0.12	0.893	2.3
Residual Error	2	8990186	8990186	4495093			19.2
Total	8	46625222					

According to Joule law, heat is generated during resistance spot welding as a result of the high electrical current flowing through the welding components can be calculated as below:

$$Q = I^2 R t \tag{1}$$

Where Q is generated heat in joules, I is welding current in Amperes, t is welding time in seconds or cycles, and R is resistance in ohms. Therefore, the welding current is the most effective parameter because it is multiplied by itself. Increasing the weld current value increases the total heat generation [25].

With the exception of trial 9, which showed complete tearing in welding sheets which means high absorbed energy and high plastic deformation, the other samples showed two types of failure, the first of which was a pullout with tearing in a metal sheet close to the tensile test machine's moving jaw and the second of which was interfacial failure as shown in Fig.18.



Fig. 18. Tensile shear samples after the test

3.2 .2 Microhardness and Microstructure Results.

The microhardness test results revealed that the FZ of both nuggets had the highest hardness, followed by the HAZ and then BM. This is because the nugget zone's center had a maximum temperature that was higher than the material's melting point, while the temperature decreased slightly away from the FZ centers. The maximum hardness for the first nugget was 383 HV, and for the second FZ, it was 341 HV. This variation in hardness values was also affected by the shunt effect phenomenon as shown in Fig.19.

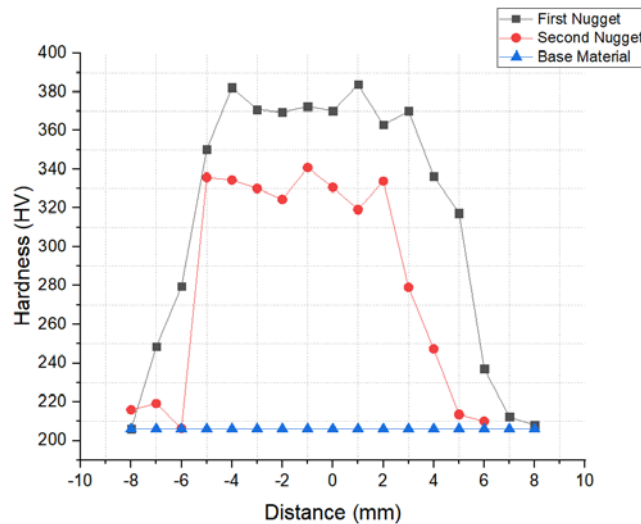


Fig. 19. Microhardness test result

The temperature in FZ that is higher than the HSLA melting point occurred to create the welding zone, followed by rapid cooling. The FZ and HAZ are heated above the critical temperature under the effect of heat produced by resistance and welding current. Ferrite begins to change into austenite and during cooling, the austenite transforms into martensite. The nugget's microstructure is made up of tiny equiaxed grains inside the nugget and columnar grains close to the fusion line (which are elongated toward the nugget zone's center). Due to the high temperatures experienced during welding and the accelerated cooling rate of higher than 1000 ° C/s, the BM microstructure changes to martensite with some bainite in the HAZ close to the fusion line. According to Figs 20, 21, and 22, the volume fraction of martensite reduced from the FZ to the BM.

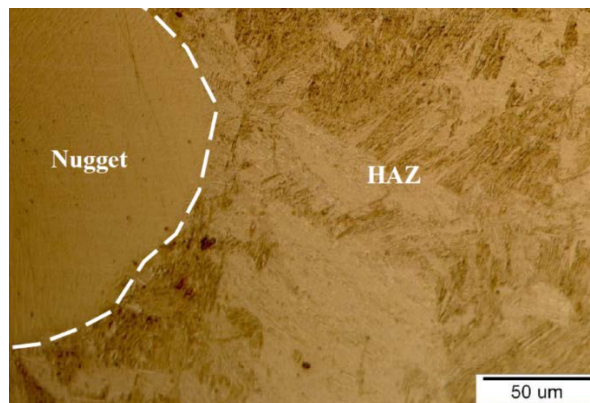


Fig. 20. An optical micrograph of the FZ/ HAZ regions

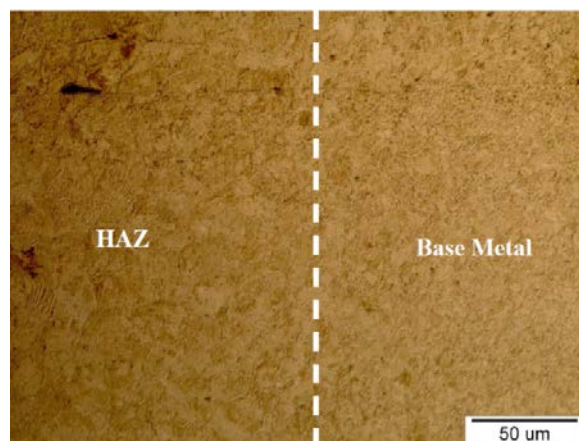


Fig. 21. Optical micrograph of the interface of HAZ and BM

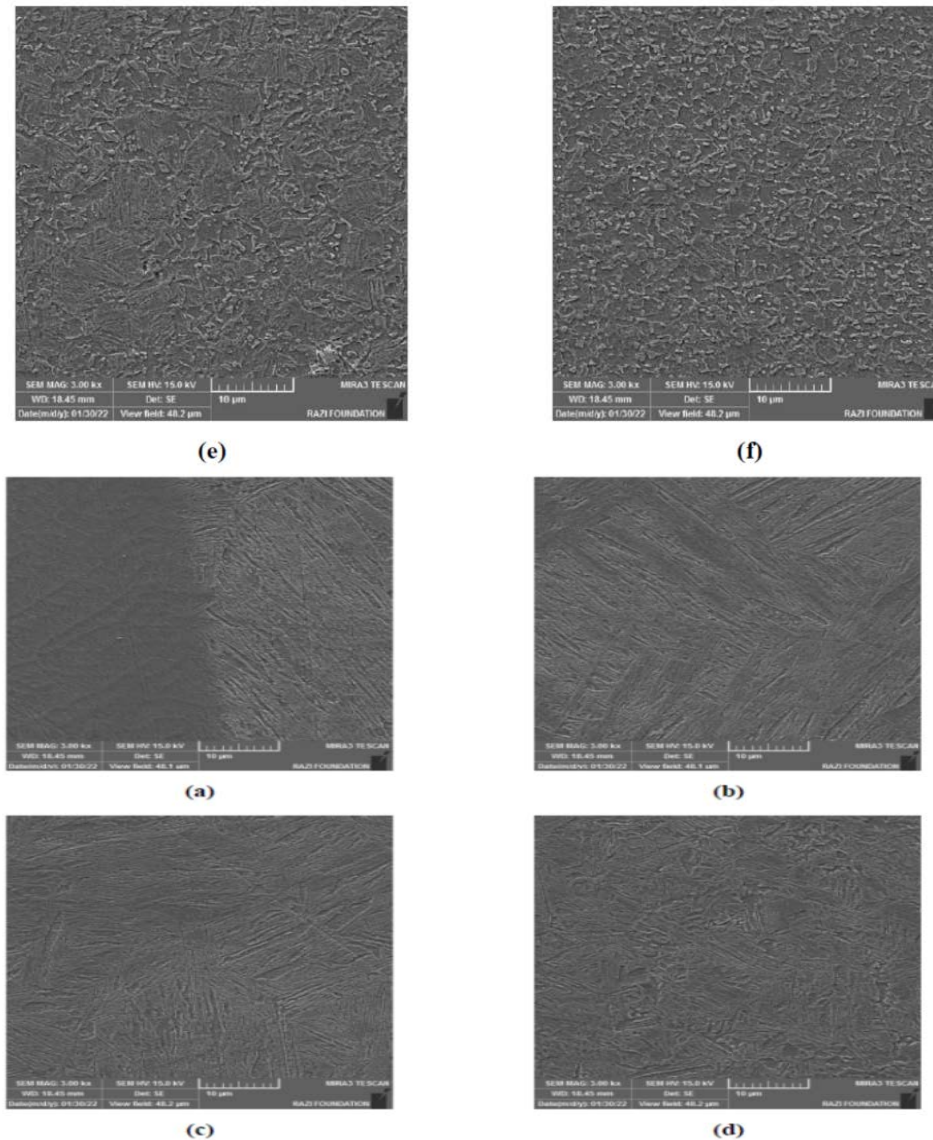


Fig. 22. FESEM test pictures from various regions: (a) FZ-HAZ interface; (b) to (e) from the HAZ towards the BM; (f) BM

3.3 Fatigue Test Results.

Fatigue life for resistance spot welding of HSLA has been examined under different loads in order to obtain the fatigue endurance limit for samples prepared with optimum welding parameters. The fatigue test started at a maximum load 15000 N with $R=0.1$ and decreased the load slowly until it reach the fatigue endurance limit which was 1500 N and it was much lower than the yield stress of HSLA steel which was 549 MPa. The fatigue life increased as the applied load decreased as summarized in table 6. Fig.23 shows the fatigue life diagram.

Table 6. Fatigue test results

Sample	Maximum Load (N)	Minimum Load (N)	Maximum Stress (MPa)	Minimum Stress (MPa)	Mean Load (N)	Amplitude Load (N)	No.of Cycles
1	15000	1500	104.5	10.5	8250	6750	505
2	13000	1300	90.5	9.05	7150	5850	2105
3	11000	1100	78	7.8	6050	4950	2720
4	9000	900	62	6.2	4950	4050	5322
5	7000	700	47.5	4.75	3850	3150	17429
6	5000	500	30.5	3.05	2750	2250	43654
7	3000	300	19.2	1.92	1650	1350	158741

Sample	Maximum Load (N)	Minimum Load (N)	Maximum Stress (MPa)	Minimum Stress (MPa)	Mean Load (N)	Amplitude Load (N)	No. of Cycles
8	2000	200	12.6	1.26	1100	900	404839
9	1500	150	9	0.9	825	675	1000000

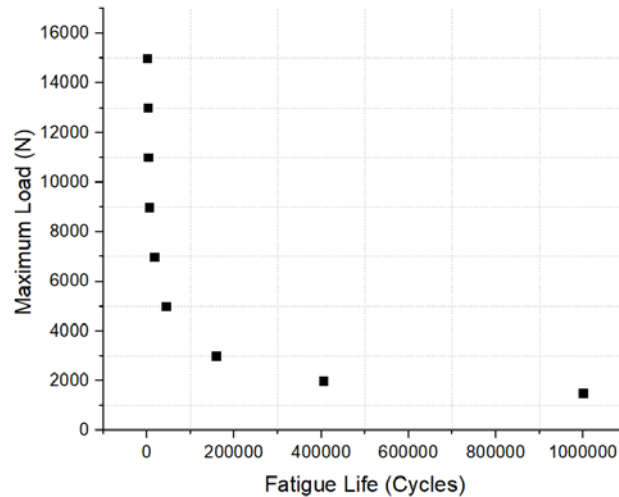


Fig. 23. Fatigue Life Diagram

Fatigue test samples showed two types of failure. For low cycle fatigue and high applied load, the failure was full pullout while for high cycle fatigue and low applied load it failed with crack propagated in HAZ and reach to BM. This occurred because of the microstructure changed in welded sample changed to brittle and formed martensite because of high welding temperature and rapid cooling as shown in Fig. 24.

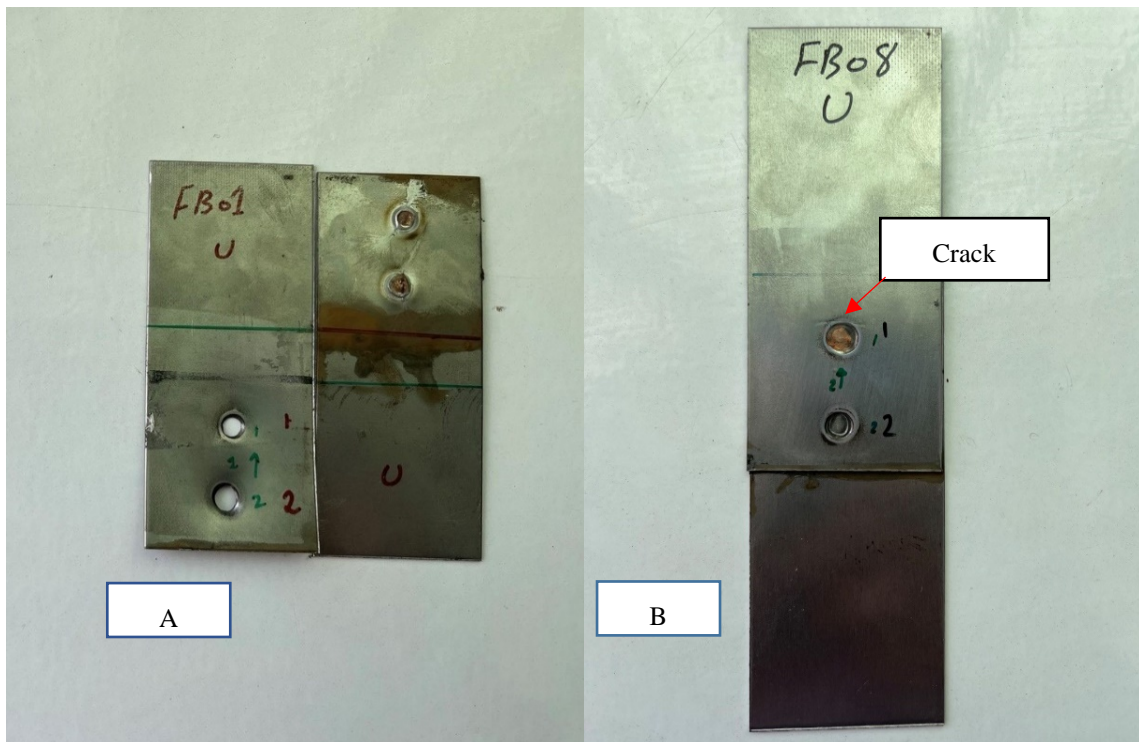


Fig. 24. (A) Low cycle fatigue sample no.1 (B) High cycle fatigue sample no. 8

4 CONCLUSIONS

This work provided a thorough analysis of RSW for high strength steel. Mechanical and microstructural tests were conducted after welding parameters were optimized. To investigate all the potential failure types that could occur with this kind of welding, fatigue tests were also conducted. The key findings can be summed up as follows:

- 1) The optimum welding current was 8800 Amp, while the optimum welding current was 30 cycles and the optimum electrode force was 2560 N and Taguchi method was a good method to achieve the optimization process.

- 2) During the tensile shear test, two types of failure happened which were interfacial failure and full tearing for the welding sheet and last one is preferred for automotive manufacturing companies because it means full absorbed energy during the crash of the cars.
- 3) The shunting effect was responsible for the variation in the nuggets' diameters, so it is advised to increase the distance between the centers of the nuggets to at least 20 mm to lessen its impact.
- 4) The maximum microhardness occurred in the center of the FZ due to high input heat and reduce slowly toward the HAZ and BM regions respectively.
- 5) The fatigue life increased as the applied load decreased until reached to endurance limit (1 million cycles) at a maximum load 1500 N.
- 6) Two types of failure showed in fatigue test which were full pullout for high load and crack propagation started from heat affected zone until reached to base material region.

5 REFERENCES

- [1] Zhang, W., Yang, S., Lin, Z., Wu, T. (2020). Weld morphology and mechanical properties in laser spot welding of quenching and partitioning 980 steel. *Journal of Manufacturing Processes*, vol.56, 1136-1145, DOI: 10.1016/j.jmapro.2020.05.057
- [2] Yang, Y.P., Gould, J., Peterson, W., Orth, F., Zelenak, P., Al-Fakir, W. (2013). Development of spot weld failure parameters for full vehicle crash modelling. *Science and Technology of Welding and Joining*.vol.18, no.3,222–231, DOI: 10.1179/1362171812Y.0000000082
- [3] Pouranvari, M., Sobhani, S., Goodarzi, F. (2018) Resistance spot welding of MS1200 martensitic advanced high strength steel: Microstructure-properties relationship. *Journal of Manufacturing Processes*, vol.31, 867-874, DOI: 10.1016/j.jmapro.2018.01.009
- [4] Li, Y.B., Li, D.L., Lin, Z.Q., David, S.A., Feng, Z., Tang, W. (2016). Review: magnetically assisted resistance spot welding. *Science and Technology of Welding and Joining*, vol.21, no.1,59–74, DOI:10.1179/1362171815Y.0000000059
- [5] Moshayedi, H., Sattari-Far, I. (2012). Numerical and experimental study of nugget size growth in resistance spot welding of austenitic stainless steels. *Journal of Materials Processing Technology*, vol.212, no.2, 347–354, DOI: 10.1016/j.jmatprotec.2011.09.004
- [6] Keeler S, (2015). Advanced high strength steels (AHSS) guidelines. Technical Report Version 4.1, World auto steel, World steel association.
- [7] R. Kuziak, R., Kawalla, R., Waegler, S. (2008). Advanced high strength steels for automotive industry. *Archives of Civil and Mechanical Engineering*, vol.8, no.2,103–117, DOI:10.1016/S1644-9665(12)60197-6
- [8] Murugan, S.P., Cheepu, M., Vijayan, V., Ji, C., Park, Y.D, (2018). The resistance spot weldability of a stainless steel/aluminium/low carbon steel 3-ply clad sheet. *Journal of Welding and Joining*, vol.36, no.1, 25–33. DOI: 10.5781/JWJ.2018.36.1.3
- [9] Sadiq, S.E., Bakhyb, S.H., Jweeg, M.J., (2020). Effects of Spot Welding Parameters on the Shear Characteristics of Aluminum Honeycomb Core Sandwich Panels in Aircraft structure. *Test engineering and management*, vol. 83, 7244 – 7255.
- [10] Jweeg, M.J., Bakhy, S.H., Sadiq, S.E., (2021). Effects of Core Height, Cell Angle and Face Thickness on Vibration Behavior of Aircraft Sandwich Structure with Honeycomb Core: An Experimental and Numerical Investigations. *Materials Science Forum*, vol. 1039, 65-85, DOI: 10.4028/www.scientific.net/MSF.1039.65.
- [11] Fakhri, M. S., Al-Mukhtar, A. M., Mahmood, I. A. (2022). Comparative Study of the Mechanical Properties of Spot Welded Joints. *Materials Science Forum*, VOL. 1079, 21-28, DOI: 10.4028/p-488xsr.
- [12] Kim, D.C., Jo, H.G., Kim, Y.M., Kang, M.J., Hwang, I., (2020). Effects of electrode face thickness on resistance spot weldability of aluminum alloy 6061. *Journal of Welding and Joining*, vol.38, no.1, 67–72, DOI: 10.5781/JWJ.2020.38.1.7
- [13] Khodabakhshi, F., Kazeminezhad, M., Kokabi, A.H., (2014) .On the failure behavior of highly cold worked low carbon steel resistance spot welds. *Metallurgical and Materials Transactions A*, vol.45, no. 3, 1376–1389, DOI: 10.1007/s11661-013-2074-3
- [14] Badkoobeh, F., Nouri, A., Hassannejad, H., Mostaan, H., (2020). Microstructure and mechanical properties of resistance spot welded dual-phase steels with various silicon contents. *Materials Science and Engineering*, vol.790, DOI: 10.1016/j.msea.2020.139703
- [15] Sheikhi, M., Jaderian, S., Mazaheri, Y., Pouranvari, M., (2020). Prediction of the failure mode of automotive steels resistance spot welds. *Science and Technology of Welding and Joining*, vol.25, no. 6, 511–517, DOI:10.1080/13621718.2020.1747765
- [16] Chen, R., Zhang, C., Lou, M., Li, Y., Carlson, B.E., (2020). Effect of Al- Si coating on Weldability of press-hardened steels. *Journal of Materials Engineering and Performance*, vol.29, no.1, 626–636. DOI:10.1007/s11665-020-04555-w.

- [17] Shandook, A.A., Hassan, S.S., (2021). An Investigation of Microwave Furnace Effects on Mechanical Properties of Standard Specimens used in Tensile and Fatigue Tests due to different type of Manufacturing. Journal of Mechanical Engineering Research and Developments, vol. 44, no. 3, 111-121.
- [18] Abbass, M.K., Ataiwi, A.H., Ameen, A., (2014). Study Fatigue Behavior of Friction Stir Welded Joints for Dissimilar Aluminum Alloys (2024 -T3 and 7020 -T6). Engineering and Technology Journal, vol.32, no.2, 439-452, DOI: 10.30684/etj.32.2A.11.
- [19] Rajarajan, C., Sivaraj, P., Sonar, T., Raja, S., Mathiazhagan, N., (2022). Resistance spot welding of advanced high strength steel for fabrication of thin-walled automotive structural frames. Forces in Mechanics, vol. 7, DOI:10.1016/j.finmec.2022.100084
- [20] Tian, J., Tao, W., Yang, S., (2022). Investigation on microhardness and fatigue life in spot welding of quenching and partitioning 1180 steel. journal of materials research and technology, vol.19, 3145-3159, DOI:10.1016/j.jmrt.2022.06.083
- [21] Hussein, S.K., Barrak, O.S., (2016). Optimization the Resistance Spot Welding Parameters of Austenitic Stainless Steel and Aluminum Alloy Using Design of Experiment Method. Engineering and Technology Journal, vol.34, no.7, 1383-1401, DOI: 10.30684/etj.34.7A.11
- [22] Kimchi, M., Phillips, D.H., (2017). Resistance Spot Welding Fundamentals and Applications for the Automotive Industry. Morgan & Claypool publishers, USA.
- [23] Minitab 19 Statistical Software (2020). [Computer software], (www.minitab.com)
- [24] Pouranvari, M., Marashi, S.P.H., (2013). Critical review of automotive steels spot welding: process, structure and properties. Science and Technology of Welding and Joining, vol.18, no.5, 361-403, DOI: 10.1179/1362171813Y.0000000120
- [25] Batista, M., Furlanetto, V., Brandi, S. D, (2020). Development of a Resistance Spot Welding Process Using Additive Manufacturing. Metals, vol.10, DOI:10.3390/met10050555

Paper submitted: 31.10.2022.

Paper accepted: 05.02.2023.

This is an open access article distributed under the CC BY 4.0 terms and conditions